The effect of rotation on Ice Shelf Water plumes

PAUL R. HOLLAND* AND DANIEL L. FELTHAM
Centre for Polar Observation and Modelling, Department of Space and Climate Physics, University College London, UK

Manuscript submitted for review on 24th June 2005

ABSTRACT

We present a model of the dynamics and thermodynamics of a plume of meltwater at the base of an ice shelf. Such plumes may become supercooled and deposit marine ice if they rise (due to the pressure decrease in the in situ freezing temperature) so the model incorporates both melting and freezing at the ice shelf base and a multiple-size-class model of frazil ice dynamics and deposition. The plume is considered in two horizontal dimensions, so we are able to realistically incorporate the influence of Coriolis forces for the first time. Rotation is extremely influential, with simulated plumes flowing in near-geostrophy due to the low friction at a smooth ice shelf base. As a result, an Ice Shelf Water plume will only rise and become supercooled (and thus deposit marine ice) if it is constrained to flow upslope by topography. This result agrees with the observed distribution of marine ice under Filchner-Ronne Ice shelf, Antarctica. Contrary to previous model results, the simulations predict that significant frazil deposition from Ice Shelf Water plumes is a transient phenomenon that is not maintained in steady state.

1. Introduction

Floating ice shelves provide an important interface between grounded ice sheets and the ocean's changing climate. It is not certain that a warming ocean will increase net basal melt from the largest shelves (Nicholls 1997), but increased oceanic melting is thought to be responsible for the thinning and collapse of smaller ice shelves around Antarctica and Greenland (Shepherd et al. 2003, 2004; Thomas 2004). The removal of mass from these shelves seems to result in acceleration and thinning of

Corresponding author address: Dr. Paul R. Holland, British Antarctic Survey, High Cross, Madingley Road, Cambridge, CB3 0ET, UK.
E-mail: p.holland@cpom.ucl.ac.uk

* Current affiliation: British Antarctic Survey, Cambridge, UK

their tributary ice streams, leading to sea level rise (De Angelis and Skvarca 2003; Joughin et al. 2004; Payne et al. 2004). Interaction between ice shelves and the ocean has a strong influence on the properties of several Antarctic water masses (Rivaro et al. 2003; Foldvik et al. 2004) which are precursors to Antarctic Bottom Water, the most prevalent water mass in the world and a key driver of the global thermohaline circulation (Orsi et al. 1999). Melting and freezing at the base of ice shelves is therefore of importance to the mass balance of the cryosphere and the circulation of the world's oceans.

Seawater's freezing temperature decreases with increasing pressure and therefore depth, so water at the surface freezing temperature (such as High Salinity Shelf Water, HSSW) becomes superheated as it descends and intrudes into a sub-shelf cavity, gaining the potential to melt the ice shelf base. The meltwater released cools and freshens the ambient seawater to form a water mass which is colder than the surface freezing temperature, known as Ice Shelf Water (ISW). This ISW subsequently flows along the base of the ice shelf under the influence of buoyancy, frictional and Coriolis forces, continually entraining the ambient seawater. If the ISW plume rises then the increase in local freezing temperature may cause it to become supercooled and start to freeze, both directly at the ice shelf base and (more efficiently) through the formation of frazil, tiny disc-shaped ice crystals. These crystals may settle out of the plume onto the ice shelf and, in combination with direct freezing and consolidation, this causes the accretion of large areas of basal marine ice. The cycle of melting at depth and refreezing in shallower areas due to freezing temperature variation is called the 'ice pump' (Lewis and Perkin 1983; Jenkins and Bombosch 1995).

The dynamics of ISW plumes have been the subject of many modeling studies (MacAyeal 1985; Hellmer and Olbers 1989; Jenkins 1991; Nøst and Foldvik 1994), but frazil ice dynamics in ISW plumes has so far only been studied by Holland and Feltham (2005) and in the one-dimensional depth-averaged models of Jenkins and Bombosch (1995) and Smedsrud and Jenkins (2004) (hereafter referred to as SJ), who produced a good spatial agreement with basal melting and freezing rates inferred from observation (Joughin and Padman 2003). The dynamics of the majority of these models are limited in that the path taken by each plume must be chosen beforehand. Payne et al. (in preparation) employ a simplified version of the model used here to examine melt rates beneath the floating section of Pine Island Glacier; no supercooling or frazil formation is predicted in that case.

ISW plumes are particularly important under Filchner-Ronne Ice Shelf (FRIS), Antarctica, the most voluminous ice shelf on Earth (Fig. 1). In winter, brine rejection from sea ice formation in the Weddell Sea generates HSSW, which sinks under FRIS and melts its grounding line at depths of up to 2000 m (Lambrecht et al. 1999). The resulting ISW plumes influence ocean properties in the cavity (Nicholls and Østerhus 2004) and lay down thick deposits of marine ice in shallower areas of the shelf (Fig. 1), redistributing the ice shelf's mass.

The aim of this paper is to examine in detail the effects of Coriolis force on an

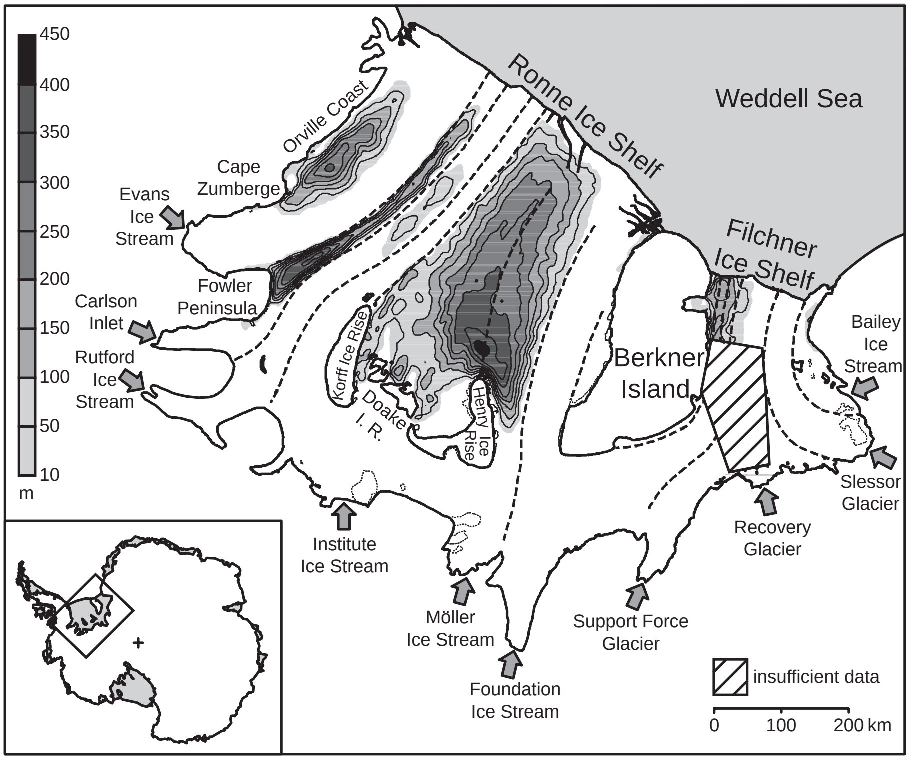

FIG. 1. Map of marine ice thickness at the base of Filchner-Ronne Ice Shelf [after Sandhäger et al. (2004)].

ISW plume. This is accomplished by incorporating frazil ice dynamics and ocean–ice shelf interaction into an unsteady plume model which is two-dimensional in the horizontal plane. We therefore consider transient effects and the full horizontal momentum balance governing ISW flow for the first time.

In the remainder of this paper, we present a discussion of the model (section 2) and a range of model results (section 3). We initiate the results section by reducing our model to a one-dimensional formulation comparable to that of SJ, so that we can test our model developments against a well-understood benchmark. Next we elucidate the basic effects of rotation on a two-dimensional plume flowing under a generalized wedge-like ice shelf topography. Finally, the model is applied to a simplified ice shelf geometry representative of the Evans Ice Stream section of FRIS (Fig. 1), where our predictions of frazil ice deposition agree with measured areas of marine ice. After examining the sensitivity of our results to variation in key parameters, we discuss (in section 4) the implications of our findings for the flow of meltwater under the rest of FRIS.

2. Mathematical Model and Simplifications

a. Model overview

The ISW plume is simulated by combining a parameterization of ice shelf basal interaction and a multiple-size-class frazil dynamics model with an unsteady, depth-averaged reduced-gravity plume model. In the model an active region of ISW evolves above and within an expanse of stagnant ambient fluid, which is considered to be ice-free and has fixed profiles of temperature and salinity. The horizontal extent of the active plume is determined by a simple 'wetting and drying' scheme based on the slope of the interface between the plume and ambient fluid (Jungclaus and Backhaus 1994).

ISW is treated as a mixture of seawater and frazil ice crystals. The frazil ice concentration C is the total ice volume per unit mixture volume and is distributed between N_{ice} size classes such that $C = \sum_{i=1}^{N_{ice}} C_i$. Frazil crystals are treated as circular discs and each class is defined by a fixed crystal radius so that growth or melting results in a transfer of mass between classes. In addition to frazil growth, melting, and precipitation, we model the process of secondary nucleation, whereby new frazil nuclei form from existing ice crystals.

U and V are depth-averaged velocities in directions x and y, which are the horizontal cross-shelf and horizontal along-shelf (parallel to glaciological flow) coordinates respectively (Fig. 2). z is the vertical coordinate, taken to be positive upwards from the sea bed near the grounding line. A and B are the positions of the ambient–plume and ice shelf–plume interfaces respectively and D is the plume depth. The ice shelf–plume interface B is treated as fixed regardless of any melting and freezing which takes place.

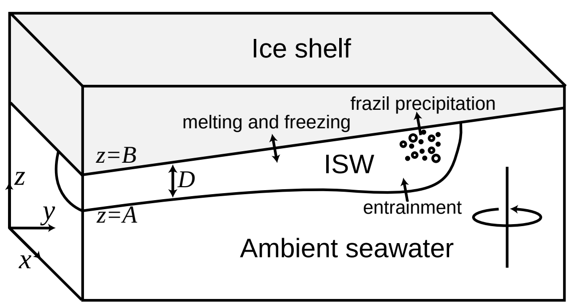

FIG. 2. Definition of coordinates and schematic of relevant processes.

To initiate the plume, we assume that basal melting at the ice shelf's grounding line due to the intrusion of HSSW generates a mixed layer of ISW with a fixed depth of $D_{in} = 5$ m. This mixed layer has the properties of a water mass made up of equal parts of the ambient seawater and the meltwater, which itself has properties calculated by considering the melting of ice in the ambient seawater according to the model of Gade (1979). The ISW is then allowed to evolve until either the plume density matches that of the ambient fluid or the plume flows out of the computational domain. In the former case the plume should separate from the shelf and flow out into the ambient fluid, processes which we are unable to model using this formulation. In the latter case we are able to continue the model run until a steady state is found for the part of the plume which remains in the domain.

b. Governing equations

The plume is considered to be a two-component mixture of ice and seawater that is treated as a homogeneous fluid with averaged properties (Jenkins and Bombosch 1995). The density of the mixture is

$$\rho_m = \rho + C(\rho_I - \rho), \tag{1}$$

where $\rho_I = 920$ kg m^{-3} is the ice density and the seawater density ρ is described by a linearized equation of state:

$$\rho = \rho_0[1 + \beta_S(S - S_0) - \beta_T(T - T_0)], \tag{2}$$

where $\rho_0 = 1030$ kg m^{-3}, $T_0 = -2.0$ °C, $S_0 = 34.5$ psu, $\beta_S = 7.86 \times 10^{-4}$ psu^{-1} and $\beta_T = 3.87 \times 10^{-5}$ °C^{-1} (Jenkins and Bombosch 1995).

Applying the Boussinesq approximation and integrating over the plume depth, we obtain conservation of mass equations for the mixture, water fraction and each ice class respectively:

$$\frac{\partial D}{\partial t} + \boldsymbol{\nabla} \cdot (D\boldsymbol{u}) = e' + m' + p', \tag{3}$$

$$\frac{\partial[(1-C)D]}{\partial t} + \boldsymbol{\nabla} \cdot [(1-C)D\boldsymbol{u}] = \boldsymbol{\nabla} \cdot [K_h D \boldsymbol{\nabla}(1-C)] + e' + m' + f', \tag{4}$$

$$\frac{\partial(C_i D)}{\partial t} + \boldsymbol{\nabla} \cdot (C_i D\boldsymbol{u}) = \boldsymbol{\nabla} \cdot (K_h D \boldsymbol{\nabla} C_i) + \frac{\rho_0}{\rho_I}(p_i' + n_i' - f_i'), \tag{5}$$

where $\boldsymbol{\nabla} = (\partial/\partial x, \partial/\partial y)$ and $\boldsymbol{u} = (U, V)$. Here e', m', p', f', and n' are the rates of entrainment, basal melting, frazil precipitation, frazil melting and frazil secondary nucleation respectively. The subscript i denotes the property of an individual frazil size class and lack of a subscript implies summation over all size classes where applicable. For consistency, all primed variables are defined as rates of seawater transport (m s^{-1}) and are positive when the plume gains mass; e', m', and f' are positive when the water fraction gains mass and p' and n' are positive when the ice fraction (or component thereof) gains mass. The horizontal eddy diffusivity for heat and salt is taken to be $K_h = 100$ m^2 s^{-1} (Gerdes et al. 1999) and we use the same diffusivity for frazil ice.

By assuming the ambient fluid to be stationary and horizontally-homogeneous and treating the pressure gradient terms according to Killworth and Edwards (1999), we obtain the depth-integrated Boussinesq Navier-Stokes equations of Jungclaus and

Backhaus (1994):

$$\frac{\partial(DU)}{\partial t}+\boldsymbol{\nabla}\boldsymbol{\cdot}(D\boldsymbol{u}U)=\boldsymbol{\nabla}\boldsymbol{\cdot}(A_h D\boldsymbol{\nabla}U)+\frac{gD^2}{2\rho_0}\frac{\partial\rho_m}{\partial x}-g'D\frac{\partial A}{\partial x}-c_d U|\boldsymbol{u}|+DfV, \quad (6)$$

$$\frac{\partial(DV)}{\partial t}+\boldsymbol{\nabla}\boldsymbol{\cdot}(D\boldsymbol{u}V)=\boldsymbol{\nabla}\boldsymbol{\cdot}(A_h D\boldsymbol{\nabla}V)+\frac{gD^2}{2\rho_0}\frac{\partial\rho_m}{\partial y}-g'D\frac{\partial A}{\partial y}-c_d V|\boldsymbol{u}|-DfU. \quad (7)$$

Here the eddy viscosity for momentum A_h is assumed to equal K_h, $g' = (\rho_m - \rho_a)g/\rho_0$ is the reduced gravity, ρ_a is the plume–ambient interface density, $g = 9.81$ m^2 s^{-1} is the gravitational acceleration and f is the Coriolis parameter. The coefficient c_d represents the drag exerted on the current by the stationary ambient fluid in addition to the drag at the ice shelf base.

Extending the scalar transport equations of SJ to an unsteady case in which horizontal turbulent diffusion of heat and salt are not negligible, we arrive at

$$\frac{\partial(DT)}{\partial t}+\boldsymbol{\nabla}\boldsymbol{\cdot}(D\boldsymbol{u}T)=\boldsymbol{\nabla}\boldsymbol{\cdot}(K_h D\boldsymbol{\nabla}T)+e'T_a+m'T_b-\gamma_T(T-T_b)-f'\left(\frac{\mathcal{L}}{c_0}-T_f\right) \quad (8)$$

and (with ice salinity set to zero)

$$\frac{\partial(DS)}{\partial t}+\boldsymbol{\nabla}\cdot(D\boldsymbol{u}S)=\boldsymbol{\nabla}\cdot(K_h D\boldsymbol{\nabla}S)+e'S_a. \quad (9)$$

Here T_a and S_a are the temperature and salinity of the ambient fluid at the plume–ambient interface, $\mathcal{L} = 3.35 \times 10^5$ J kg^{-1} is the latent heat of ice fusion and $c_0 = 3974$ J kg^{-1} °C^{-1} is the specific heat capacity of seawater. T_f is the pressure freezing temperature at the mid-depth of the plume, T_b is the temperature at the interface between ice shelf and ocean and γ_T is a diffusion coefficient representing the transfer of heat in the adjacent boundary layer.

c. Entrainment

The entrainment parameterization used in previous ISW plume models is a simplified version of the formula derived by Bo Pederson (1980) for steam-tube models. Jungclaus and Backhaus (1994) found that a more realistic behavior throughout a horizontally-varying plume could be achieved by using the Kochergin (1987) formulation, which explicitly represents the relative strengths of shear production and stability suppression of turbulence:

$$e' = \frac{c_l^2}{\mathrm{Sc}_T}\sqrt{(U^2+V^2)\left(1+\frac{\mathrm{Ri}}{\mathrm{Sc}_T}\right)}, \quad (10)$$

where $\mathrm{Ri} = g'D/(U^2+V^2)$ is the Richardson number and we choose $c_l = 0.012$ on the basis that this value produces a plume which becomes supercooled and deposits frazil ice in the correct position (see section 3c). The turbulent Schmidt number Sc_T

is given by the formula of Mellor and Durbin (1975):

$$\mathrm{Sc}_T = \frac{\mathrm{Ri}}{0.0725\left(\mathrm{Ri} + 0.186 - \sqrt{\mathrm{Ri}^2 - 0.316\mathrm{Ri} + 0.0346}\right)}. \tag{11}$$

d. Drag

The choice of drag coefficient is important because in this model friction is the only force which breaks geostrophy and causes flow across isobaths (Jungclaus and Backhaus 1994). Form drag at the sea bed is usually simulated in numerical ocean models by adopting the quadratic drag terms in (6) and (7) with a c_d value of order 10^{-3}, matching values inferred from observation (Ramming and Kowalik 1980). In contrast, simplified plume models applied to idealized 'wedge' bathymetries require c_d to be orders of magnitude larger in the rotating case in order to force the plume to flow downslope far enough to match observations (Killworth 1977; Bo Pederson 1980; Jungclaus and Backhaus 1994). The model adopted here has been used to demonstrate that quantitatively correct downslope propagation can be achieved with $c_d = 3 \times 10^{-3}$ if a realistic bathymetry is used (Jungclaus and Backhaus 1994; Jungclaus et al. 1995).

Unfortunately, the basal roughness of ice shelves is currently an unknown quantity. Previous authors have used a drag coefficient of 2.5×10^{-3}, a choice which can be traced back to early examination of the roughness of grassland on Salisbury Plain in England (Taylor 1920; Ramming and Kowalik 1980; MacAyeal 1984, 1985).

Despite basal crevassing, ice shelf bases are generally thought to be smooth due to the effects of melting and ice pumping. For this reason, the drag coefficient at an ice shelf base should be lower than those used to represent the seabed, so the value of 1.5×10^{-3} adopted by Holland and Jenkins (1999) and Holland and Feltham (2005) is used here. In section 3c of this study we demonstrate that this value is reasonable by fitting the deposition zone of our predicted plume to observations of basal freezing (Joughin and Padman 2003) and marine ice deposition patterns (Sandhäger et al. 2004). We note, however, that there exist instability mechanisms which could cause corrugations to form on the underside of an ice shelf (Ashton and Kennedy 1972; Feltham and Worster 1999); insufficient information is available to quantify these effects at this time.

e. Basal melting and freezing

To calculate the basal melt rate m', we formulate balances of heat and salt at the ice shelf–plume boundary (Jenkins and Bombosch 1995):

$$m' \frac{\mathcal{L}}{c_0} = \gamma_T (T - T_b), \tag{12}$$

$$m' S_b = \gamma_S (S - S_b), \tag{13}$$

where S_b is the interface salinity, γ_S is the salt diffusion coefficient in the boundary layer, and for simplicity we have assumed that diffusion of heat into the ice shelf is negligible. The interface quantities T_b and S_b are constrained by a linearized pressure freezing temperature relation (also used for T_f):

$$T_b = a S_b + b + c\zeta_b \tag{14}$$

where $a = -0.0573$ °C psu^{-1}, $b = 0.0832$ °C, and $c = -7.61 \times 10^{-4}$ °C m^{-1} and ζ_b is the depth of the ice shelf base below sea level (Jenkins and Bombosch 1995). Equations (12) - (14) are combined to solve for m' and thus T_b. The diffusion coefficients are given by

$$\gamma_T = \frac{c_d^{1/2} |\boldsymbol{u}|}{2.12 \ln(c_d^{1/2} |\boldsymbol{u}| D/\nu_0) + 12.5 \, \mathrm{Pr}^{2/3} - 9}, \tag{15}$$

$$\gamma_S = \frac{c_d^{1/2} |\boldsymbol{u}|}{2.12 \ln(c_d^{1/2} |\boldsymbol{u}| D/\nu_0) + 12.5 \mathrm{Sc}^{2/3} - 9}, \tag{16}$$

where $\nu_0 = 1.95 \times 10^{-6}$ m^2 s^{-1} is the molecular viscosity, $\mathrm{Pr} = 13.8$ is the molecular Prandtl number, and Sc $= 2432$ is the molecular Schmidt number of seawater (Jenkins and Bombosch 1995).

f. Frazil nucleation

When the plume has risen far enough for the increasing in situ freezing point to make it supercooled, frazil ice will nucleate and grow. Ice nuclei must be fairly abundant under ice shelves, since the maximum observed supercooling there is only 0.035 °C (Nicholls and Jenkins 1993; Nicholls et al. 2004), but the exact process of nucleation is uncertain. We follow SJ in assuming that dendrite-like platelet ice crystals growing on the ice shelf base may be detached by eddies and suspended in the water column, providing frazil nuclei of a range of sizes. However, we are unable to adopt the exact nucleation strategy of SJ because our model is unsteady and multi-dimensional.

Our frazil nucleation logic is as follows: If a model cell is newly supercooled (i.e. it was not supercooled on the previous time step), we set the concentration of each frazil class in that cell to $C_{Si} = 10^{-7}$, unless it already exceeds that value. We are therefore assuming not only that nuclei always exist, but also that they are distributed evenly over a range of sizes.

g. Frazil melting and freezing

Melting and freezing of frazil is modeled by the transfer of a certain number of ice crystals from class i to the size class above $(i+1)$ or below $(i-1)$. Therefore, the rate of change of ice concentration in each size class is determined by the difference in growth (melting) rates between that class and the class below (above). Transfer processes between classes must also be consistent with the movement of crystals of the appropriate volume (SJ). Therefore, composing f_i' from ice growth (G_i) and melting (M_i) terms (s^{-1}) and integrating over depth, we obtain

$$f_i' = \frac{\rho_I D}{\rho_0}\left\{\frac{v_i}{\Delta v_i}\left[(1-H)M_{i+1} + HG_i\right] - \frac{v_i}{\Delta v_{i-1}}\left[(1-H)M_i + HG_{i-1}\right]\right\}, \tag{17}$$

where v_i is the volume of a crystal in the ith size class, $\Delta v_i = v_{i+1} - v_i$ and $H = \mathrm{He}(T_f - T)$ is the Heaviside step function (Holland and Feltham 2005).

Under the assumptions that growth of frazil in turbulent seawater occurs only at the disc edge, is controlled by the heat flux rather than salinity, and has the disc radius as the appropriate length scale for the temperature gradient, we formulate growth as

$$G_i = \frac{c_0 \mathrm{Nu}_i K_T}{\mathcal{L}}(T_f - T)\frac{2}{r_i^2}C_i \tag{18}$$

and, assuming that melting occurs over the whole crystal surface, melting is

$$M_i = \frac{c_0 \mathrm{Nu}_i K_T}{\mathcal{L}}(T_f - T)\frac{2}{r_i}\left(\frac{1}{r_i} + \frac{1}{2a_r r_i}\right)C_i \tag{19}$$

(SJ). In these expressions Nu_i is the Nusselt number for each size class, $K_T = 1.4 \times 10^{-7}$ m^2 s^{-1} is the molecular thermal diffusivity, and r_i and $a_r = 0.02$ are the radius and aspect ratio of frazil discs respectively (SJ). We follow Hammar and Shen (1995) in allowing Nu_i to vary with ice crystal size:

$$\mathrm{Nu}_i = \begin{cases} \frac{1}{m_i^*} + 0.17\,\mathrm{Pr}^{1/2} & m_i^* \leqslant \frac{1}{\mathrm{Pr}^{1/2}} \\ \frac{1}{m_i^*} + 0.55\left(\frac{\mathrm{Pr}}{m_i^*}\right)^{1/3} & m_i^* > \frac{1}{\mathrm{Pr}^{1/2}} \end{cases}, \tag{20}$$

where $m_i^* = r_i/\eta$ is the ratio between the disc radius and the Kolmogorov length scale.

h. Frazil secondary nucleation

Secondary nucleation is the process whereby new frazil crystal nuclei are detached from ‘parent’ crystals. In this study the formulation of Svensson and Omstedt (1994) is adopted, whereby collision between crystals is assumed to be the detachment mechanism and a proportion of the ice crystals in each size class are converted to ‘nuclei’ (crystals in the smallest class) according to the frequency of crystal collision. The rate of secondary nucleation is proportional to the number of crystal collisions in the volume swept by all crystals in unit time:

$$n_1' = \frac{\rho_I D}{\rho_0} \sum_{i=2}^{N_{ice}} \pi \tilde{n} \frac{W_i}{r_i^e} r_1^{e3} C_i, \tag{21}$$

$$n_{i\neq 1}' = -\frac{\rho_I D \pi \tilde{n}}{\rho_0} \frac{W_i}{r_i^e} r_1^{e3} C_i, \tag{22}$$

where $\tilde{n}$ is the average number of ice crystals of all sizes per unit volume, subject to a maximum value of 10^3, and r_i^e is an effective radius of frazil discs, equal to the radius of a sphere with the same volume as a disc of radius r_i. W_i represents the ice crystal velocity along a path which incorporates both buoyant rising and turbulent motions:

$$W_i^2 = w_i^2 + \frac{4\epsilon}{15\nu_0} r_i^{e2}, \tag{23}$$

where $\epsilon = 7.4 \times 10^{-6}$ W kg^{-1} is the turbulent dissipation rate and the frazil rise velocity w_i relative to the moving fluid is approximated by frazil's buoyant drift velocity in still water (Gosink and Osterkamp 1983).

i. Frazil precipitation

To represent frazil deposition onto the ice shelf, we adopt the Jenkins and Bombosch (1995) adaptation of the sedimentation parameterization of McCave and Swift (1976), which assumes that the flux of crystals depositing under buoyancy is reduced by turbulence in the boundary layer:

$$p_i' = -\frac{\rho_I}{\rho_0} w_i C_i \left(1 - \frac{|\boldsymbol{u}|^2}{U_{Ci}^2}\right) \mathrm{He} \left(1 - \frac{|\boldsymbol{u}|^2}{U_{Ci}^2}\right). \tag{24}$$

In this expression U_{Ci} is a critical plume velocity for each size class above which no precipitation can occur and the Heaviside function prevents any erosion from taking place.

3. Results

In this section we begin by reducing the model to a version which reproduces the results of SJ, and then introduce our model developments one at a time in order to reveal their modifications to the conclusions of earlier work. Boundary conditions for these simulations are no-slip and zero scalar flux at all solid walls and zero gradients otherwise. A high spatial and temporal resolution was required to achieve grid- and time step-independence, particularly in the modeling of frazil, so a grid resolution of 250 m and a time step of 10 s were adopted throughout. Whenever a simulation includes rotation a latitude of 78°S is used.

a. One-dimensional model

To match the results of SJ, we consider a non-rotating ice shelf with a base which is uniform in the y direction and adopt a uniform plume inflow along the length of the grounding line, thus removing all forcings from the model which could lead to variation in that direction. We match our model to their 'linear ice shelf' case, in which the shelf base rises uniformly from a grounding line at 1400 m depth to an ice front at 285 m depth a distance of 600 km away. The ambient fluid has properties appropriate for the ocean cavity under FRIS: a salinity profile which decreases linearly from 34.71 psu at the grounding line depth to 34.5 psu at the surface and a temperature rising linearly from $-2.18°$C at the grounding line to $-1.9°$C at the surface (Jenkins and Bombosch 1995). Our frazil size classes have radii of 0.01, 0.05, 0.15, 0.3, 0.4, 0.5, 0.6, 0.8, 1 and 2 mm. We use an inflow of pure meltwater (Gade 1979) with a depth of $D_{in} = 1$ m. We set $A_h = K_h = 0, c_d = 2.5 \times 10^{-3}$, and $\mathrm{Nu}_i = 1$ to mimic their parameter choices and we re-adopt their frazil seeding strategy, in which the supercooled cell nearest to the grounding line has the frazil concentration fixed to $C_{Si} = 4 \times 10^{-9}$. The features distinguishing the two models are then transience (SJ use a steady-state model) and the formulation of buoyancy forcing and entrainment. We modify the latter by setting $q = 0.01775$, which matches e' to its counterpart in SJ according to Jungclaus and Backhaus (1994). Figure 3a shows the results of this model after 75 days, when the plume first separates from the ice shelf. This situation is taken to be analogous to the steady state of SJ and the frazil concentrations match theirs well. Seeding takes place at 410 km from the inflow, effectively providing an upstream boundary condition for each frazil class. The total concentration increases with distance downstream because the crystals grow as they move through the supercooled region.

Switching the frazil seeding formulation to our new strategy but keeping the seed population at $C_{Si} = 4 \times 10^{-9}$, we obtain the results shown in Fig. 3b at plume separation. Frazil is seeded at the head of the current as it passes and subsequently grows in response to the crystal dynamics rather than the advection of a fixed upstream population. One consequence of this is that the frazil grows further from the inflow, while the plumes themselves propagate similar distances (as revealed by the thick lines in Fig. 3).

Figures 3c and 3d show results from our full frazil model, which has the new seeding strategy with $C_{Si} = 10^{-7}$ and also uses the Hammar and Shen (1995) formulation for Nu_i [Eq. (20)]. The latter change has a rather small effect but the new seeding results in a significant increase in frazil concentrations, creating a more buoyant plume which separates later at 80 days. Another feature of note is that there is a greater concentration of frazil in the smaller size classes; the larger seeding prevents the limitation of growth by a shortage of smaller crystals, a feature of the frazil model discussed fully in Holland and Feltham (2005).

The effects of the changes to the frazil precipitation caused by different seeding

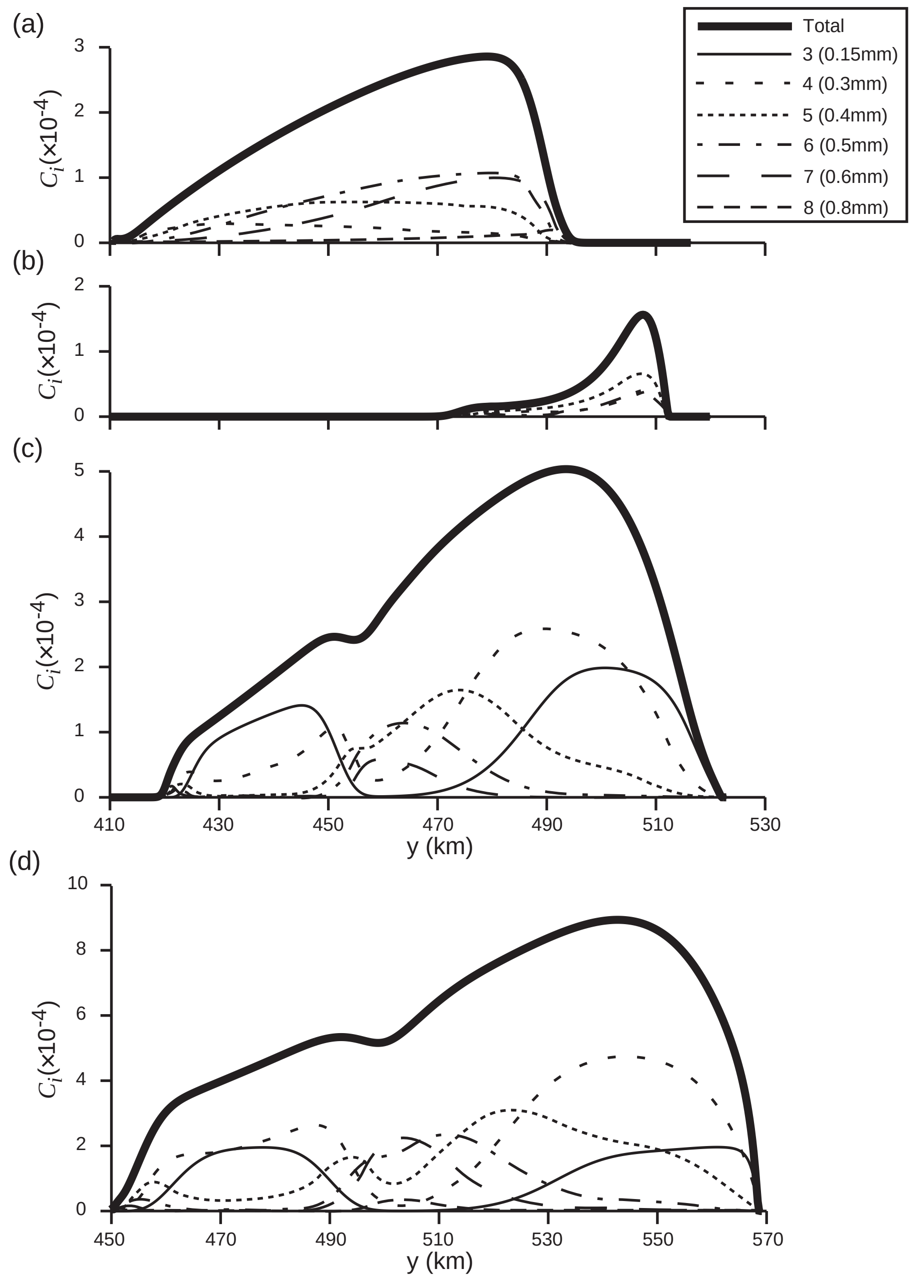

FIG. 3. Frazil ice concentrations resulting from various seeding strategies in one-dimensional simulations. (a) SJ seeding strategy after 75 days, (b) our seeding strategy and $C_{Si} = 4 \times 10^{-9}$ after 75 days, (c) our seeding strategy after 75 days, (d) our seeding strategy after 80 days. In each case the thick line also shows the extent of the plume. Note the different scales in (d).

formulations are of interest here because they have a bearing on our later claims for the model. Figures 4a and 4b show the frazil precipitation predicted by both SJ and our model at the point of separation using SJ's seeding formulation. The results of our SJ-matching model compare well with the original (Fig. 4b), although our precipitation has a sharper profile, which we attribute to the high spatial and temporal resolution used in this study. A more important difference is that we predict the precipitation of larger frazil crystals than SJ. This occurs because our plume flows slightly faster than theirs (due to the more sophisticated formulation of buoyancy terms) and its speed exceeds the critical velocity for precipitation of frazil in classes 5 and 6.

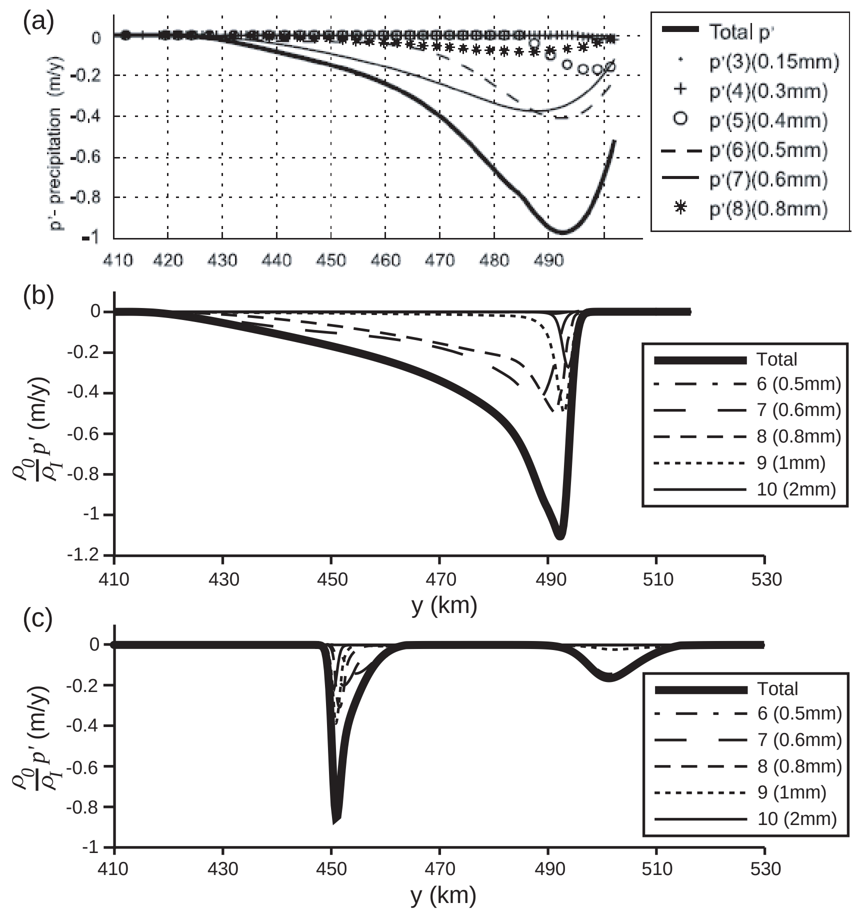

FIG. 4. Frazil precipitation rates (m year^{-1}) in the one-dimensional simulations. (a) Steady-state results from SJ, (b) results of our SJ-matching model after 75 days, (c) results of our chosen model after 80 days.

Precipitation in our model using our revised seeding formulation (Fig. 4c) has a similar magnitude but qualitatively different spatial character to SJ's results. The most important area of precipitation is at the rear of the supercooled region, where the largest crystals are located. This is the area which was seeded first and has been supercooled for the longest time, so the frazil population contains larger crystals which precipitate more readily.

b. Idealized two-dimensional model

To elucidate the basic two-dimensional behavior of ISW plumes, in this section the full model described in section 2 is used with a wedge-shaped ice shelf. All of the model simplifications of the previous section are removed, but we keep the same ambient fluid properties and frazil size classes. The plume starts from an initial mixed layer of width $W_{in} = 10$ km under an ice shelf which rises from 1100 m depth at the grounding line to 500 m depth at a distance of 200 km downstream. This domain geometry is chosen to be representative of the slope of Evans Ice Stream (Fig. 1), as discussed in section 3c. All boundaries are considered to be open apart from on the inflow side, where solid walls represent the grounding line. The modeled plumes do not separate from the ice shelf, so the steady-state results occur after the head of each gravity current has left the domain. In this section we show 'snapshots' of results after 30 days of simulation.

Figure 5a shows the plume thickness in the non-rotating case. The plume flows directly up the shelf with a speed of approximately 8 cm s^{-1} and tapers from a thick head at the propagating plume front to a shallow plume near the inflow. Model experiments show that frazil concentrations similar to those reported in section 3a can be produced down the centerline of a non-rotating plume of this type.

Figure 5b demonstrates the effect of adding Coriolis terms to the momentum balance of a simulation which is otherwise identical to that of Fig. 5a. The flow is nearly geostrophic because basal drag is so low, so Coriolis forces immediately deflect the plume until it flows almost parallel to isobaths of the ice shelf base. The plume flows much more slowly under this new balance (approximately 2 cm s^{-1}) and it does not propagate far upslope from the inflow region. If ISW plumes do not flow upslope they will not become supercooled or produce any marine ice.

As discussed in section 2d, this tendency for a model plume to flow alongslope is in contradiction to observations (when a reasonable drag coefficient is used) and is partly due to the neglect of realistic bathymetric features in the model domain (Jungclaus and Backhaus 1994). In addition, this depth-averaged model neglects the details of flow in an Ekman layer next to the ice shelf in which viscous forces are important and upslope 'draining' of fluid should occur (Cenedese et al. 2004). These effects can be partly reproduced by increasing the drag coefficient to $c_d = 1.5 \times 10^{-2}$ from the standard value of $c_d = 1.5 \times 10^{-3}$, and Fig. 5c shows that this does indeed make the plume flow further up the slope than before.

c. Evans Ice Stream model

In this section we attempt to model the flow of meltwater underneath the Evans Ice Stream section of FRIS (Fig. 1) and thereby explain the origin of the region of marine ice located near Cape Zumberge. Satellite observations imply that vigorous

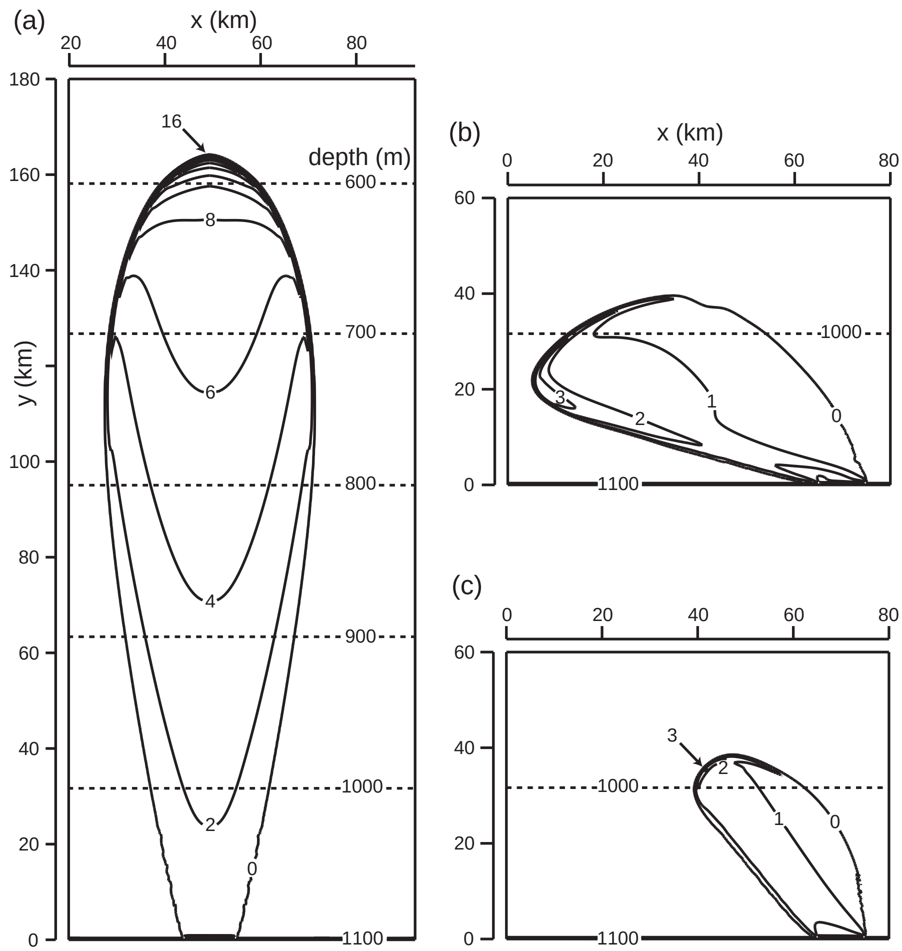

FIG. 5. Contours of plume thickness (m) in the various cases after 30 days of simulation. (a) No rotation, (b) rotation, (c) rotation and high basal drag ($c_d = 1.5 \times 10^{-2}$).

melting occurs near the grounding line of Evans Ice Stream (Joughin and Padman 2003) so as before we consider the evolution of a plume from a 10 km-wide inflow which represents a layer of mixed meltwater and ambient. The domain is the same as before apart from a wall running perpendicular to the grounding line, which represents the 135 km-long boundary between Evans Ice Stream inlet and Cape Zumberge. The Cape itself is represented as a quarter-circle with radius 35 km (Fig. 6). The topography of the ice shelf base is set such that its isobaths are perpendicular to the wall everywhere, a situation roughly approximating the real bathymetry in this location (Sandhäger et al. 2004).

The modeled ISW plume does not separate from the shelf, so we examine its properties after 80 days of simulation. The plume immediately turns left from the grounding line under the influence of Coriolis forces, but is impeded by the wall and forced to propagate upslope instead, becoming a very narrow boundary current

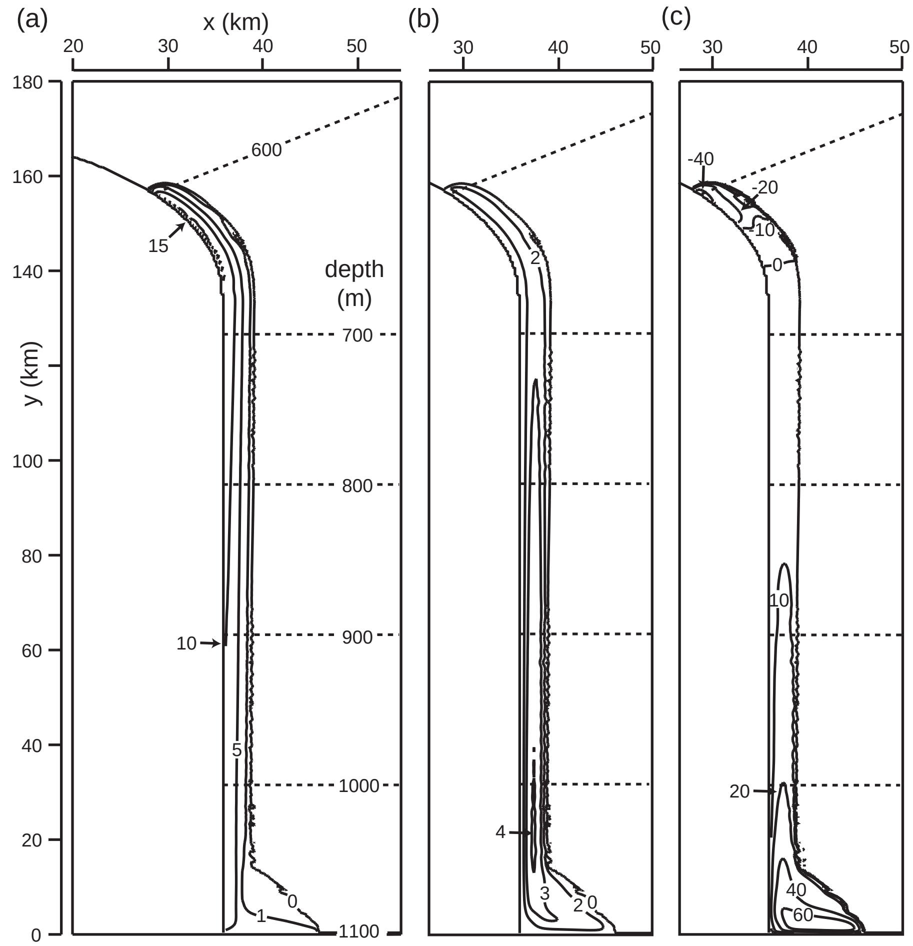

FIG. 6. Results of the Evans Ice Stream case (a rotating plume constrained by a wall) after 80 days. (a) Plume thickness D (m), (b) plume speed $|\boldsymbol{u}|$ (cm s^{-1}), (c) total basal mass transfer $\frac{\rho_0}{\rho_I}(m' + p')$ (cm year^{-1}). Note that all plots are stretched in the x direction. The 600 m shelf base isobath marked in (a) represents the section used to assess model sensitivity in Table 1.

with the ISW banked up against the wall (Fig. 6a). The plume moves slightly more quickly than the geostrophic plume (Fig. 5b) but is still much slower than a non-rotating plume due to the retarding influence of drag from the no-slip wall.

Figure 6c shows that we predict a basal melting of up to 60 cm year^{-1}, a frazil precipitation rate of up to 50 cm year^{-1}, and a direct freezing rate of up to 1 cm year^{-1}; according to our model, frazil overwhelmingly dominates direct freezing as a source of marine ice. Comparing these results to Fig. 1, the deposition area of marine ice off Cape Zumberge is reproduced rather well considering our simplified bathymetry. However, it is important to note the transient behavior of the model. Frazil forms in the head of the plume when it becomes supercooled on first approaching the corner in the wall, after traveling 130 km in 65 days. The moving head of the

Simulation	Day	W (m)	$\bar{D}$ (m)	$\lvert\boldsymbol{u}\rvert$ (cm s^{-1})	Melt (m^3 y^{-1})	Freeze (m^3 y^{-1})	Precipitation (m^3 y^{-1})
Reference	81	3.26	7.15	1.69	78×10^6	-0.4×10^6	-8×10^6
$c_l = 0.01$	86	3.26	7.08	1.45	56×10^6	-0.4×10^6	-10×10^6
$c_l = 0.014$	78	3.40	7.67	1.88	100×10^6	-0.2×10^6	-3×10^6
$c_d = 1.5 \times 10^{-4}$	92	3.26	7.07	1.46	46×10^6	-2×10^3	-64×10^3
$c_d = 1.5 \times 10^{-2}$	115	3.61	8.11	0.84	71×10^6	-5×10^6	-30×10^6
$A_h = K_h = 50$ m^2 s^{-1}	58	2.70	7.58	2.44	111×10^6	0	0
$A_h = K_h = 150$ m^2 s^{-1}	102	3.82	7.30	1.34	61×10^6	-0.5×10^6	-22×10^6
$W_{in} = 5$ km	97	3.05	5.12	1.39	35×10^6	-0.2×10^6	-4×10^6
$W_{in} = 15$ km	74	3.61	8.66	1.90	126×10^6	-0.7×10^6	-9×10^6
$D_{in} = 2.5$ m	97	3.05	5.31	1.44	59×10^6	-0.1×10^6	-3×10^6
$D_{in} = 10$ m	64	3.82	10.33	2.17	115×10^6	-0.9×10^6	-13×10^6
Meltwater inflow	69	3.61	9.60	1.90	61×10^6	-0.7×10^6	-11×10^6

Table 1. Model sensitivity to variation in parameters relating to the physics of the plume. The reference simulation has $c_l = 0.012$, $c_d = 1.5 \times 10^{-3}$, $A_h = K_h = 100$ m^2 s^{-1}, $W_{in} = 10$ km, and $D_{in} = 5$ m. All results are taken from the first day after the head of the plume has passed the 600 m ice shelf base isobath and W, $\bar{D}$ and $\lvert\bar{\boldsymbol{u}}\rvert$ are taken across that section (as shown in Fig. 6a). Basal melt (freeze) is the total volume transfer to (from) the plume at that time.

gravity current remains the position of greatest frazil concentration throughout the whole simulation. The plume continues to flow and precipitate along the wall after traversing Cape Zumberge. This means that we do not find a steady state in which significant precipitation occurs in any fixed location. Supercooling and frazil formation continue at the corner of Cape Zumberge once the plume head has passed, but with a maximum precipitation rate of only 2 cm year^{-1}.

d. Sensitivity studies

In this section we consider the sensitivity of our model results to variation in the parameters of the model (Table 1), focusing on those relating to the dynamics of the plume rather than the frazil model formulation, which was closely examined by SJ and in section 3a.

Increasing the entrainment of ambient fluid into the plume by increasing c_l widens and thickens the plume, accelerating it due to the relative decrease in the importance of drag. The extra entrainment causes more melting to occur and reduces the amount of marine ice deposition by increasing the superheating and enlarging the area of the plume over which melting takes place. Decreasing c_l has the opposite effect.

Varying the basal drag produces slightly more complex results. The plume speed is reduced when the drag is both raised and lowered; in the former case the basal drag simply impedes motion and in the latter case the tendency of the plume to flow upslope is reduced so that the plume is confined closer to the no-slip wall and lateral drag becomes even more important. In both cases the total melt is reduced due to a decrease in the size of the melting region. In the low-drag case the narrower and slower plume melts a smaller area less vigorously, becoming supercooled further from the inflow and thus depositing a smaller volume of marine ice. In the high-drag case the plume becomes supercooled closer to the inflow, so an increase in the total marine ice production accompanies the decrease in melting. This happens because the entrainment (which suppresses supercooling) is primarily a function of the plume velocity and is thus decreased relative to the melting, which also depends upon the increased drag through the transfer coefficients (15) and (16).

Increasing the eddy viscosity A_h and eddy diffusivity of heat, salt, and frazil K_h smooths horizontal density gradients and widens the plume, making the gradient of the ambient–plume interface shallower. Both effects decelerate the plume by reducing the buoyancy forcing, which results in less melting and greater marine ice production. This occurs because the entrainment responds nonlinearly to changes in velocity (via the velocity-dependence of the turbulent Schmidt number) while the basal melting formulation responds almost linearly; decelerating the plume by reducing its buoyancy decreases the entrainment more than the melting, the plume becomes supercooled sooner as a result, and reduced melting and increased freezing rates ensue. The opposite is true for decreased A_h and K_h.

Since rotation banks the plume up against the wall, increasing the depth of the inflow has a similar effect to increasing its width. Either way, increasing the inflow volume makes the plume deeper, decreasing the overall influence of drag and thus accelerating the plume. The acceleration increases basal melting and freezing and also increases frazil precipitation by producing more supercooling. The nonlinearity of the increase in entrainment detailed in the previous paragraph is diminished by the thickening of the plume (this offsets the velocity-driven increase in Ri which raises Sc_T).

The 'meltwater inflow' case has the properties of the initial mixed layer set to pure ice shelf meltwater rather than equal parts of meltwater and ambient seawater. This accelerates the plume due to the larger density difference between the plume and ambient, but reduces melting at the ice shelf base because there is less available superheating in the plume. The plume becomes supercooled sooner and refreezing and frazil precipitation are increased.

4. Discussion

The effect of rotation on ISW plumes has been demonstrated by systematically adding components to a one-dimensional non-rotating model used by previous authors. Our final case of a wall-bounded rotating plume predicts ice deposition patterns which generally account for the observed distribution of marine ice near Cape Zumberge in Fig. 1. These results also qualitatively match basal melting and freezing rates inferred from satellite observation (Joughin and Padman 2003). However, both of these data sources suggest that our plume adheres to the coastline too closely in the frazil deposition zone. Joughin and Padman (2003) show an area of refreezing stretching approximately 100 m from Cape Zumberge, and in Fig. 1 marine ice thickness increases in the direction of glaciological flow (implying ice deposition) over the same area. In addition Nicholls et al. (2004) find supercooled fluid approximately 13 km from the Western wall near the front of Ronne Ice Shelf. Our plume's deposition zone is narrower than these observations, but we would have to adopt the full shelf base profile to test whether our simplified shelf bathymetry is responsible for this. Another possibility is that the frazil deposition off Cape Zumberge might partly result from a meltwater source other than the grounding line of Evans Ice Stream. In this study we have chosen not to include an exact bathymetry or multiple meltwater sources in favor of a simplified study elucidating the basic properties of rotating ISW plumes.

The model predicts melt, precipitation, and freeze rates of 60 cm year^{-1}, 50 cm year^{-1}, and 1 cm year^{-1} respectively. These rates agree well with other modeling studies (SJ, Jenkins and Holland 2002a,b), but are under-predicted by an order of magnitude according to Joughin and Padman (2003). Joughin and Padman (2003) concede that their radar altimeter shelf thicknesses might be less accurate near the grounding line, so it is possible that they overestimate melt there. Marine ice is thought to form from consolidation of the layers of frazil slush observed near the ice shelf base (Nicholls and Jenkins 1993; Nicholls et al. 2004), the rate of which is probably governed by the rate of brine rejection from the slush. Frazil precipitation rates are therefore not directly comparable to marine ice accretion rates. In addition, our parameterization of direct basal freezing takes no account of this consolidation process, and assumes that the freezing surface is flat rather than a tortuous crystal matrix or slush. To truly compare models to observed basal accretion rates we require a better understanding of the process of marine ice consolidation.

Contrary to previous studies, the model predicts that a high frazil deposition rate is a transient phenomenon which does not persist indefinitely. A small area of frazil deposition occurs off Cape Zumberge throughout the simulation but large precipitation rates only occur as the plume's head passes. This further exacerbates the problem of our low predicted refreezing rates, since the rates of Joughin and Padman (2003) are calculated in steady state. Our model suggests that ISW plumes are essentially a transient phenomena, which is supported by the idea that seasonal pulses of HSSW sink under the ice shelf and intermittently melt ice at the grounding line (Nicholls 1996). Our model shows that an ISW pulse would take around 80 days to traverse the first part of the ice shelf and initiate refreezing. There is no evidence with which to test this time scale, but 4 cm s^{-1} seems to be a reasonable current speed under FRIS in general (Nicholls and Østerhus 2004).

We find that Coriolis forces are an important influence on ISW plumes, implying that they will only become supercooled if steered by an obstruction running perpendicular to isobaths of the ice shelf base. This concept explains the distribution of marine ice under FRIS (Fig. 1); Cape Zumberge, Fowler Peninsula, Korff Ice Rise and Doake Ice Rumples all channel meltwater upslope and account for the nearby freezing zones. We postulate that the significant area of marine ice in the center of Ronne Ice Shelf is a result of both Henry Ice Rise and the large sub-shelf ridge emanating from Foundation Ice Stream steering meltwater from the east, possibly including sections of the grounding line of Filchner Ice Shelf. The refreezing under Filchner Ice Shelf could either originate from melting immediately south of Berkner Island or from grounding line melt steered in the channels in the base of Filchner Ice Shelf.

A natural progression of our study is to incorporate the exact bathymetry of FRIS and quantitatively determine the source region and freezing rate for each area of marine ice. However, several aspects of the model warrant further investigation. The detailed structure of the Ekman layer could be represented, as this affects downslope drainage. The processes involved in plume separation could be modeled, although there is little experimental or observational data for this. The slush layer and its consolidation process could be represented in the parameterization of direct basal freezing. Finally, very little is known about the melting at grounding lines which provides the initial impetus for these plumes. Despite these shortcomings, the model presented in this study is realistic enough for us to be confident in its emphasis of the important effects of rotation on ISW plumes.

Acknowledgments. We are grateful to Johann Jungclaus for allowing us to examine the source code for his plume model and to Henner Sandhäger for the map of marine ice thickness.

REFERENCES

Ashton, G. D., and Kennedy, J. F., 1972: Ripples on the underside of river ice covers. *J. Hydraul. Div., Proc. ASCE*, **HY9**, 1603–1624.

Bo Pederson, F., 1980: Dense bottom currents in rotating ocean. *J. Hydraul. Div. Am. Soc. Civ. Eng.*, **106**, 1291–1308.

Cenedese, C., Whitehead, J. A., Ascarelli, T. A., and Ohiwa, M., 2004: A dense current flowing down a sloping bottom in a rotating fluid. *J. Phys. Oceanogr.*, **34**, 188–203.

De Angelis, H., and Skvarca, P., 2003: Glacier surge after ice shelf collapse. *Science*, **299**, 1560–1562.

Feltham, D. L., and Worster, M. G., 1999: Flow-induced morphological instability of a mushy layer. *J. Fluid Mech.*, **391**, 337–357.

Foldvik, A., Gammelsrød, T., Østerhus, S., Fahrbach, E., Rohardt, G., Schröder, M., Nicholls, K. W., Padman, L., and Woodgate, R. A., 2004: Ice shelf water overflow and bottom water formation in the southern Weddell Sea. *J. Geophys. Res.*, **109**, C02015, doi:10.1029/2003JC002008.

Gade, H. G., 1979: Melting of ice in sea water; a primitive model with application to the Antarctic ice shelf and icebergs. *J. Phys. Oceanogr.*, **9**, 189–198.

Gerdes, R., Determann, J., and Grosfeld, K., 1999: Ocean circulation beneath Filchner-Ronne Ice Shelf from three-dimensional model results. *J. Geophys. Res.*, **104**, 15 827–15 842.

Gosink, J. P., and Osterkamp, T. E., 1983: Measurements and analyses of velocity profiles and frazil ice-crystal rise velocities during periods of frazil-ice formation in rivers. *Ann. Glaciol.*, **4**, 79–84.

Hammar, L., and Shen, H. T., 1995: Frazil evolution in channels. *J. Hydraul. Res.*, **33**, 291–306.

Hellmer, H. H., and Olbers, D. J., 1989: A two-dimensional model for the thermohaline circulation under an ice shelf. *Antarc. Sci.*, **1**, 325–336.

Holland, D. M., and Jenkins, A., 1999: Modelling thermodynamic ice–ocean interactions at the base of an ice shelf. *J. Phys. Oceanogr.*, **29**, 1787–1800.

Holland, P. R., and Feltham, D. L., 2005: Frazil dynamics and precipitation in a water column with depth-dependent supercooling. *J. Fluid Mech.*, **530**, 101–124, doi:10.1017/S002211200400285X.

Jenkins, A., 1991: A one-dimensional model of ice shelf–ocean interaction. *J. Geophys. Res.*, **96**, 20 671–20 677.

Jenkins, A., and Bombosch, A., 1995: Modelling the effects of frazil ice crystals on the dynamics and thermodynamics of Ice Shelf Water plumes. *J. Geophys. Res.*, **100**, 6967–6981.

Joughin, I., Abdalati, W., and Fahnestock, M., 2004: Large fluctuations in speed on Greenland's Jakobshavn Isbræ glacier. *Nature*, **432**, 608–610.

Joughin, I., and Padman, L., 2003: Melting and freezing beneath Filchner-Ronne Ice Shelf, Antarctica. *Geophys. Res. Lett.*, **30**, 1477, doi:10.1029/2003GL016941.

Jungclaus, J. H., and Backhaus, J. O., 1994: Application of a transient reduced gravity plume model to the Denmark Strait outflow. *J. Geophys. Res.*, **99**, 12 375–12 396.

Jungclaus, J. H., Backhaus, J. O., and Fohrmann, H., 1995: Outflow of dense water from the Storfjord in Svalbard: a numerical model study. *J. Geophys. Res.*, **100**, 24 719–24 728.

Killworth, P. D., 1977: Mixing on the Weddell Sea continental slope. *Deep-Sea Res.*, **24**, 427–448.

Killworth, P. D., and Edwards, N. R., 1999: A turbulent bottom boundary layer code for use in numerical ocean models. *J. Phys. Oceanogr.*, **29**, 1221–1238.

Kochergin, V. P., 1987: Three-dimensional prognostic models. *Three-dimensional coastal ocean models, Coastal Estuarine Stud. Ser.*, No. 4, Amer. Geophys. Union, 201–208.

Lambrecht, A., Meyer, C., Oerter, H., and Nixdorf, U., 1999: Investigations of the mass balance of the southeastern Ronne Ice Shelf, Antarctica. *Ann. Glaciol.*, **29**, 250–254.

Lewis, E. L., and Perkin, R. G., 1983: Supercooling and energy exchange near the Arctic Ocean surface. *J. Geophys. Res.*, **88**, 7681–7685.

MacAyeal, D. R., 1984: Numerical simulations of the Ross Sea tides. *J. Geophys. Res.*, **89**, 607–615.

MacAyeal, D. R., 1985: Evolution of tidally triggered meltwater plumes below ice shelves. *Oceanology of the Antarctic continental shelf, Antarc. Res. Ser.*, No. 43, Amer. Geophys. Union, 133–143.

McCave, I. N., and Swift, S. A., 1976: A physical model for the rate of deposition of fine-grained sediments in the deep sea. *Geol. Soc. Am. Bull.*, **87**, 541–546.

Mellor, G. L., and Durbin, P. A., 1975: The structure and dynamics of the ocean surface mixed layer. *J. Phys. Oceanogr.*, **5**, 718–728.

Nicholls, K. W., 1996: Temperature variability beneath Ronne Ice Shelf, Antarctica, from thermistor cables. *J. Geophys. Res.*, **101**, 1199–1210.

Nicholls, K. W., 1997: Predicted reduction in basal melt rates of an Antarctic ice shelf in a warmer climate. *Nature*, **388**, 460–462.

Nicholls, K. W., and Jenkins, A., 1993: Temperature and salinity beneath Ronne Ice Shelf, Antarctica. *J. Geophys. Res.*, **98**, 22 553–22 568.

Nicholls, K. W., Makinson, K., and Østerhus, S., 2004: Circulation and water masses beneath the northern Ronne Ice Shelf, Antarctica. *J. Geophys. Res.*, **109**, C12017, doi:10.1029/2004JC002302.

Nicholls, K. W., and Østerhus, S., 2004: Interannual variability and ventilation timescales in the ocean cavity beneath Filchner-Ronne Ice Shelf, Antarctica. *J. Geophys. Res.*, **109**, C04014, doi:10.1029/2003JC002149.

Nøst, O. A., and Foldvik, A., 1994: A model of ice shelf–ocean interaction with application to the Filchner-Ronne and Ross Ice Shelves. *J. Geophys. Res.*, **99**, 14 243–14 254.

Orsi, A. H., Johnson, G. C., and Bullister, J. L., 1999: Circulation, mixing, and production of Antarctic

Bottom Water. *Prog. Oceanogr.*, **43**, 55–109.

Payne, A. J., Vieli, A., Shepherd, A. P., Wingham, D. J., and Rignot, E., 2004: Recent dramatic thinning of largest West Antarctic ice stream triggered by oceans. *Geophys. Res. Lett.*, **31**, L23401, doi:10.1029/2004GL021284.

Ramming, H.-G., and Kowalik, Z., 1980: *Numerical modelling of marine hydrodynamics*. Elsevier, 369pp.

Rivaro, P., Frache, R., Bergamasco, A., and Hohmann, R., 2003: Dissolved Oxygen, NO and PO as tracers for Ross Sea Ice Shelf Water overflow. *Antarc. Sci.*, **15**, 399–404.

Sandhäger, H., Vaughan, D. G., and Lambrecht, A., 2004: Meteoric, marine and total ice thickness maps of Filchner-Ronne-Schelfeis, Antarctica. *Forum for Research into Ice Shelf Processes Report No. 15*, Bjerknes Centre for Climate Research, 23–29.

Shepherd, A. P., Wingham, D. J., Payne, A. J., and Skvarca, P., 2003: Larsen ice shelf has progressively thinned. *Science*, **302**, 856–859.

Shepherd, A. P., Wingham, D. J., and Rignot, E., 2004: Warm ocean is eroding West Antarctic Ice Sheet. *Geophys. Res. Lett.*, **31**, L23402, doi:10.1029/2004GL021106.

Smedsrud, L. H., and Jenkins, A., 2004: Frazil ice formation in an Ice Shelf Water plume. *J. Geophys. Res.*, **109**, C03025, doi:10.1029/2003JC001851.

Svensson, U., and Omstedt, A., 1994: Simulation of supercooling and size distribution in frazil ice dynamics. *Cold Reg. Sci. Technol.*, **22**, 221–233.

Taylor, G. I., 1920: Tidal friction in the Irish Sea. *Philos. Trans. Roy. Soc. London A*, **220**, 1–33.

Thomas, R. H., 2004: Force-perturbation analysis of recent thinning and acceleration of Jakobshavn Isbræ, Greenland. *J. Glaciol.*, **50**, 57–66.

Generated with ametsocjmk.cls.
Written by J. M. Klymak
mailto:jklymak@coas.oregonstate.edu
http://pender.coas.oregonstate.edu/WorkTools.html